Electronic Supplementary Material (ESI) for Chemical Science.

Supporting Information

Turning it off! Disfavouring hydrogen evolution to enhance selectivity for CO production during homogeneous CO_2 reduction by cobalt-terpyridine complexes

Noémie Elgrishi, Matthew B. Chambers and Marc Fontecave*

Laboratoire de Chimie des Processus Biologiques, UMR 8229 CNRS, UPMC Univ Paris 06, Collège de France, 11 Place Marcelin Berthelot, 75231 Paris Cedex 05, France.

marc.fontecave@college-de-france.fr

Index *Page*

Figure S1	$E°(Co^{II}/Co^{I})$ and $E°(Co^{I}L/Co^{I}L^{\bullet-})$ *vs.* Hammett parameter for **1**-**5**	3
Figure S2	Bulk electrolysis of **3** in the presence of acetic acid	4
Figure S3	CVs of tpy in DMF and of $CoCl_2$ in DMF	5
Figure S4	CVs of ratios of $CoCl_2$ and tpy in the presence of acetic acid	5
Figure S5	Sample *FOWA* of the catalytic activity of **3** for H_2 evolution	6
Figure S6	Values for k_1 obtained through the *FOWA* for H^+ reduction by **3** as a function of scan rate and acid concentration	6
Figure S7	CVs of **3** in DMF, $TBAPF_6$ 0.1M, under Ar, with and without 20, 40 and 60 mM acetic acid	7
Figure S8	CVs of **1**, **2**, **4** and **5** in DMF, $TBAPF_6$ 0.1M, under Ar, with and without 60 mM acetic acid	8
Figure S9	CVs of **1**-**5** in DMF/H_2O (95:5), $TBAPF_6$ 0.1M under Ar	9
Figure S10	CVs of **1**-**5** in DMF/H_2O (95:5), $TBAPF_6$ 0.1M under CO_2	9
Figure S11	Estimated k_1 for CO_2 reduction by **1**-**5** using the *FOWA*	10
Figure S12	Evolution of E during the electrolyses of **1**-**5** under CO_2 at I=-300µA	11
Figure S13	Faradic yields for H_2 and CO evolution by **1**-**5** under CO_2 at I=-300µA	12
Figure S14	Order in **5** in steady-state bulk electrolysis CO_2 reduction conditions	13
Figure S15	Schematic representation of the electrochemical cell for electrolyses	14
Figure S16	Evaluation of Rate Determining Step	15-16

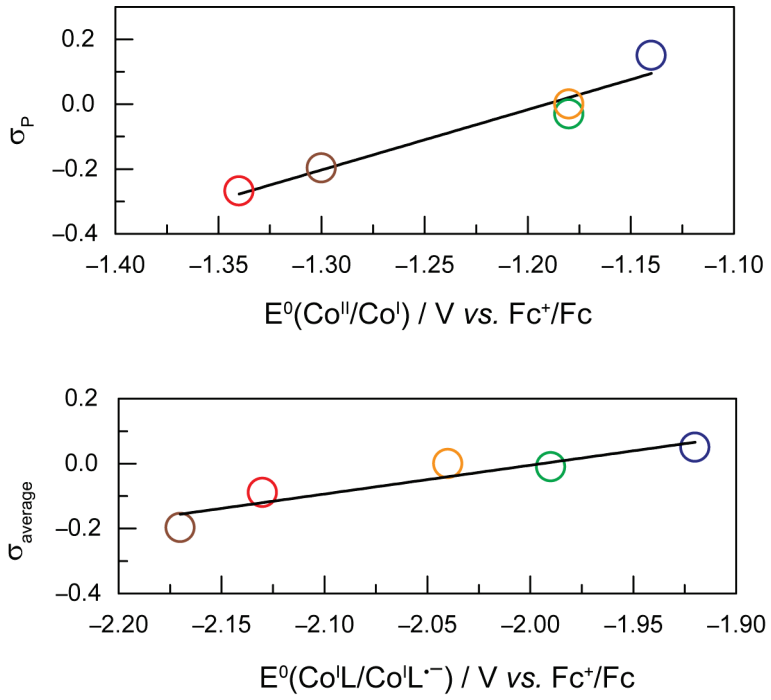

Figure S1. Top: Standard potential observed for the Co^{II}/Co^{I} couple for compounds **1** (blue), **2** (green), **3** (yellow), **4** (red) and **5** (brown) in DMF, $TBAPF_6$ 0.1M as a function of the Hammett parameter of the substituent present on *para* position of the central pyridine ring.

Bottom: Standard potential observed for the $Co^{I}L/Co^{I}L^{\bullet -}$ couple for compounds **1** (blue), **2** (green), **3** (yellow), **4** (red) and **5** (brown) in DMF, $TBAPF_6$ 0.1M as a function of the average Hammett parameters of the substituent present on the *para* position of the 3 pyridine ring.

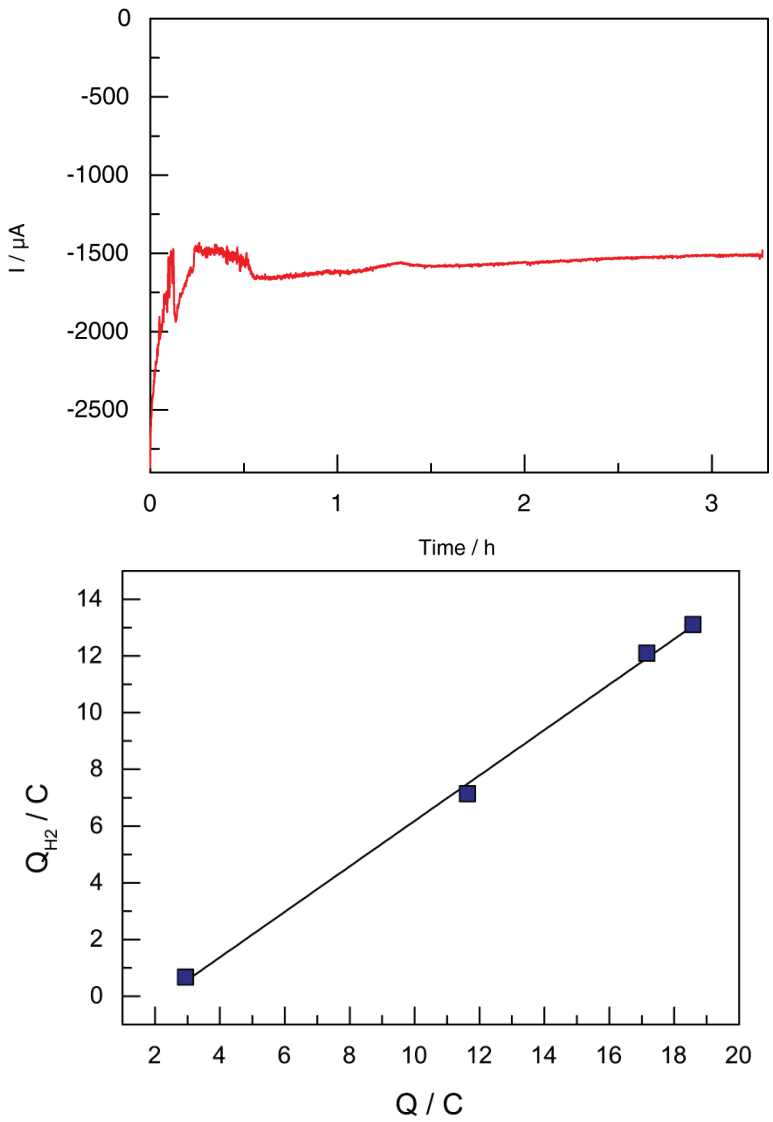

Figure S2. Top: Current (red) measured during a controlled-potential electrolysis of a 2 mM DMF solution of **3** at –2.03 V *vs.* Fc^+/Fc. The 8 mL solution of DMF, with 0.1 M of $TBAPF_6$ as supporting electrolyte and 2 M acetic acid is N_2-saturated prior to electrolysis. The bulk electrolysis cell, described in Figure S15, uses a 1.5 cm diameter pool of mercury as the working electrode. Data was recorded every 0.02 s and the current intensity data was smoothed using an adjacent-averaging method over 10 s.

Bottom: Charge corresponding to the amount of H_2 (Q_{H2}, ■ blue squares) measured in the headspace during bulk electrolysis *vs.* the total charge passed during the electrolysis. The slope of the linear fit, corresponding to the faradic efficiency, is 80%.

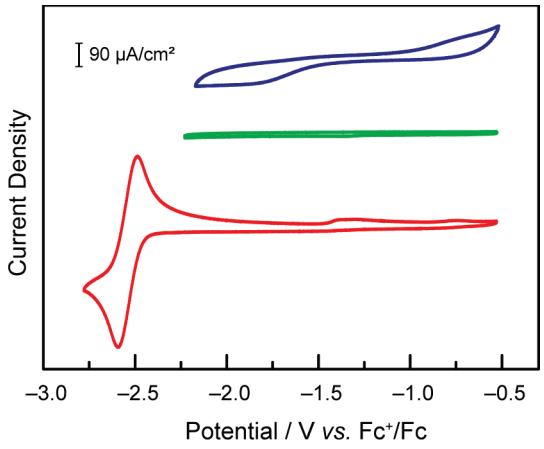

Figure S3. Cyclic voltammograms under Ar at 100 mV/s in DMF, $TBAPF_6$ 0.1M, on a glassy carbon electrode of : 1 mM $CoCl_2$ (— blue), 2 mM tpy (— green), 2 mM tpy in a wider range (— red). No wave is observed in the –1.40 V *vs.* Fc^+/Fc region.

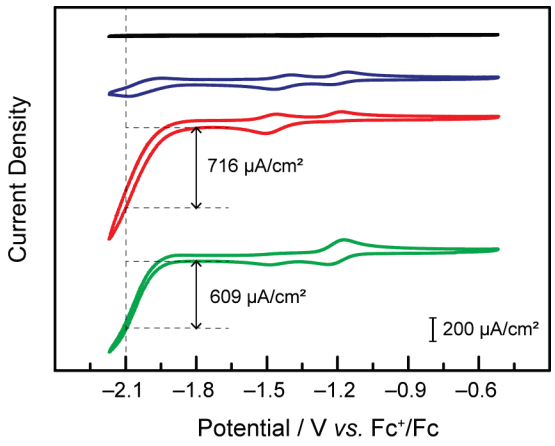

Figure S4. Cyclic voltammograms under Ar at 100 mV/s in DMF, $TBAPF_6$ 0.1M, on a glassy carbon electrode of 1 mM tpy (— black). To this solution, 1 mM $CoCl_2$ is added (— blue), followed by 40 mM of acetic acid (— red), and finally 1 mM tpy (— green).

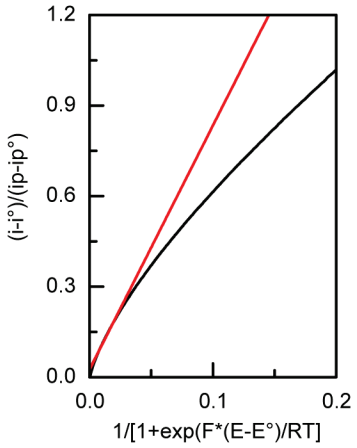

Figure S5. Sample *FOWA* of the catalytic activity of **3** for H_2 evolution, using data in Figure S7 at 500 mV/s and a concentration of acetic acid of 60 mM. The experimental data (black) is fitted linearly near the foot of the catalytic wave. The slope of the linear fit (red, slope = 8.0841, R^2=0.998) allows for determination of the rate constant k_1 following the equation:

$$slope = \frac{2\sqrt{k_{obs}}}{0.4463}\sqrt{\frac{RT}{Fv}} \text{ with } k_{obs} = k_1 \times C_A^0$$

Which here gives: $k_1 = \frac{slope^2(0.4463)^2 Fv}{4RT} \times \frac{1}{C_A^0}$ = 1056 $M^{-1}.s^{-1}$.

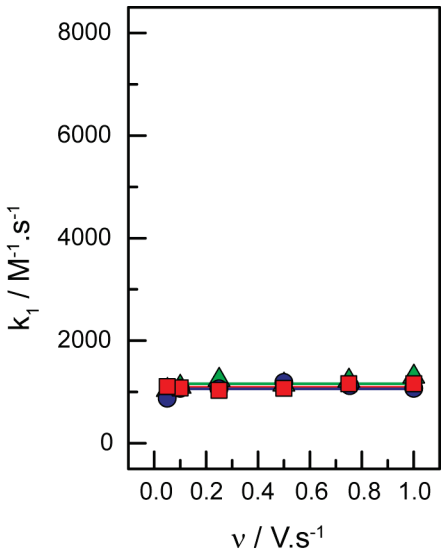

Figure S6. Values for k_1 for H^+ reduction obtained through the *FOWA* of compounds **3** using the data obtained with 20 (— green), 40 (— blue) and 60 (— red) mM of acetic acid at different scan rates. The CVs used are presented in Figure S7.

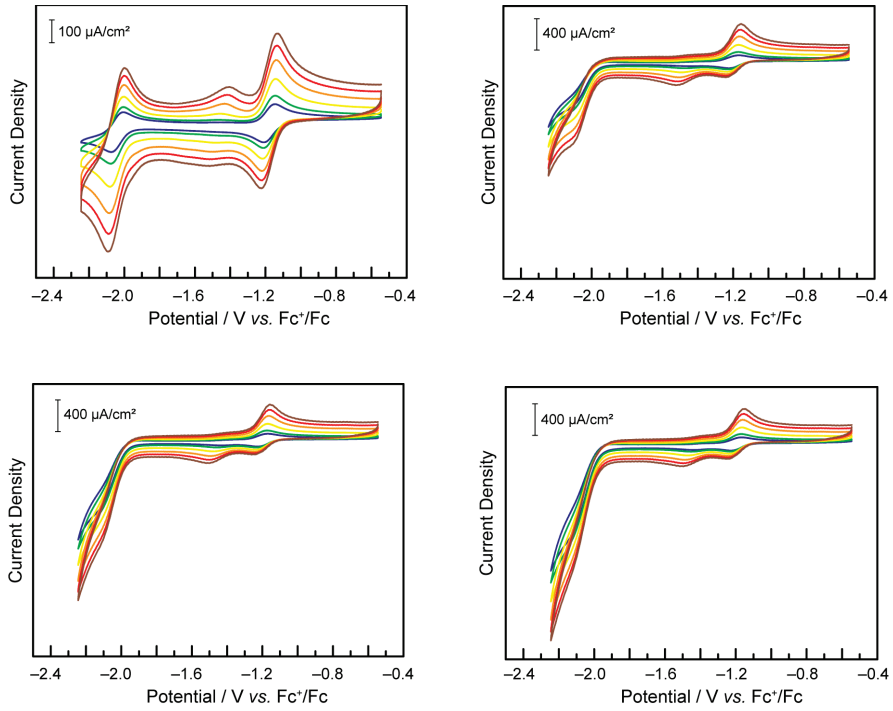

Figure S7. Cyclic voltammograms under Ar of a 1 mM solution of compound **3** in DMF, $TBAPF_6$ 0.1M, on a glassy carbon electrode without (top left) and with 20 mM (top right), 40 mM (bottom left) and 60 mM (bottom right) acetic acid at a scan rate of 50 (— blue), 100 (— green), 250 (— yellow), 500 (— orange), 750 (— red) and 1000 (— brown) mV/s. The presence of the feature around −1.4 V is only observed at fast scan rates. It is speculated to originate from a Co-*mono*tpy species.

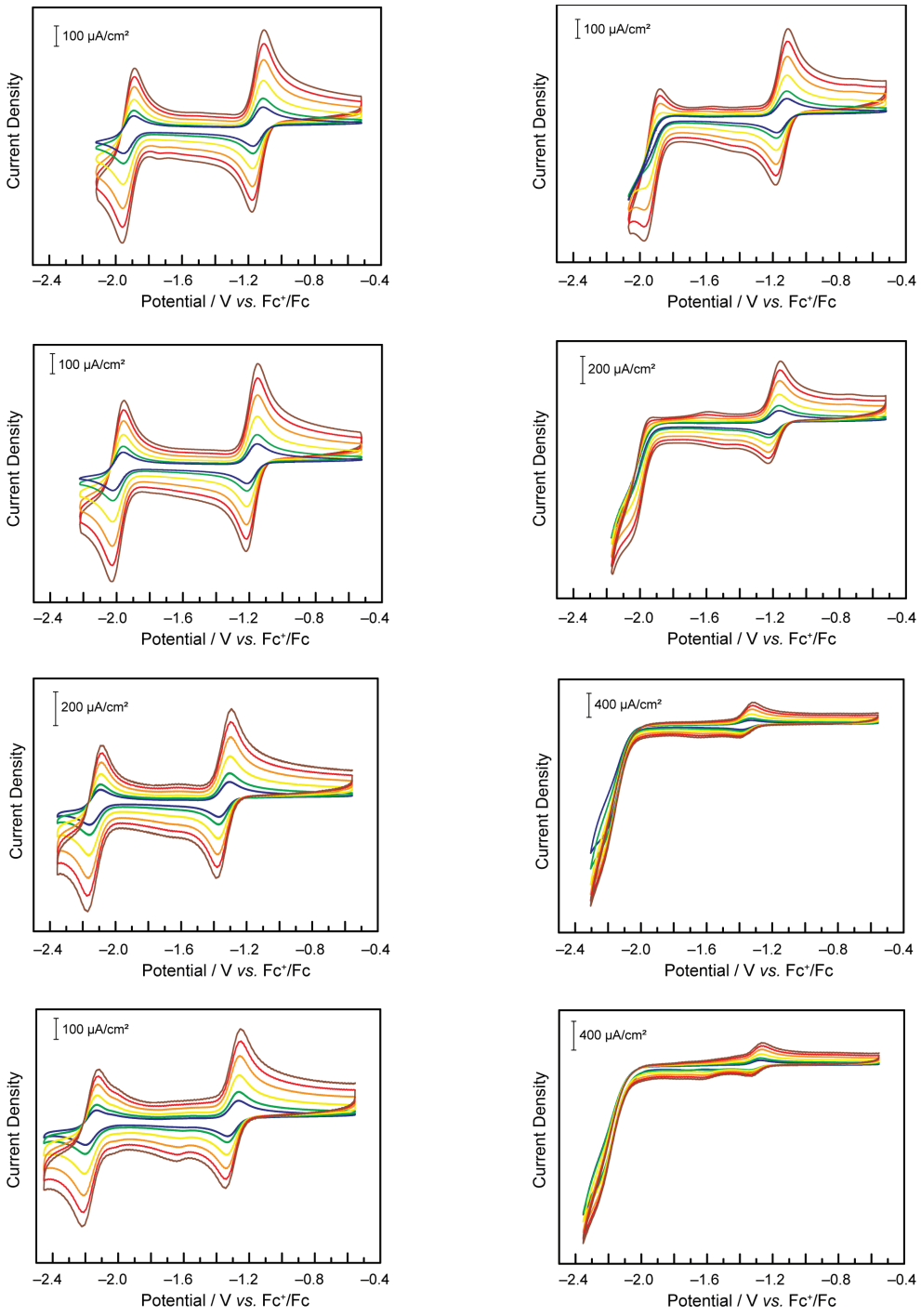

Figure S8. Cyclic voltammograms under Ar of 1 mM solutions of **1**, **2**, **4** and **5** (top to bottom), in DMF, $TBAPF_6$ 0.1M, on a glassy carbon electrode without (left) and with (right) 60 mM acetic acid at a scan rate of 50 (— blue), 100 (— green), 250 (— yellow), 500 (— orange), 750 (— red) and 1000 (— brown) mV/s.

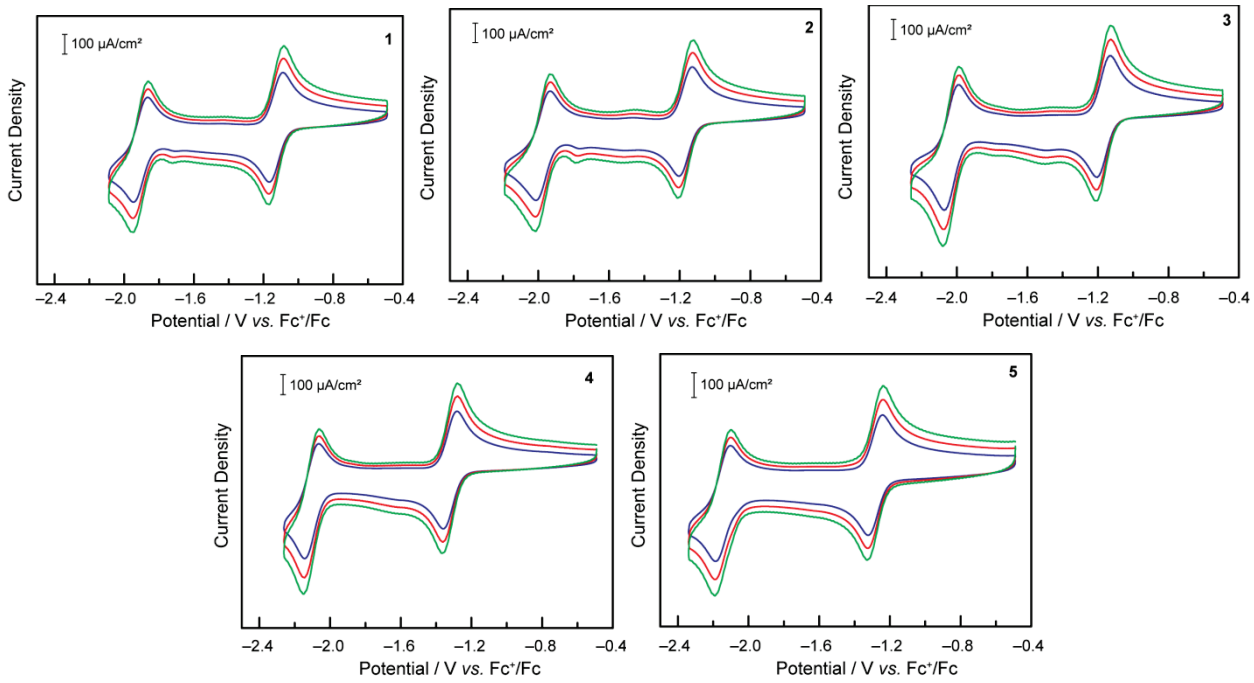

Figure S9. Cyclic voltammograms of 1 mM solutions of **1**, **2**, **3**, **4** and **5** in DMF/H_2O (95:5), $TBAPF_6$ 0.1M, on a glassy carbon electrode under Ar at a scan rate of 500 (— blue), 750 (— red) and 1000 (— green) mV/s.

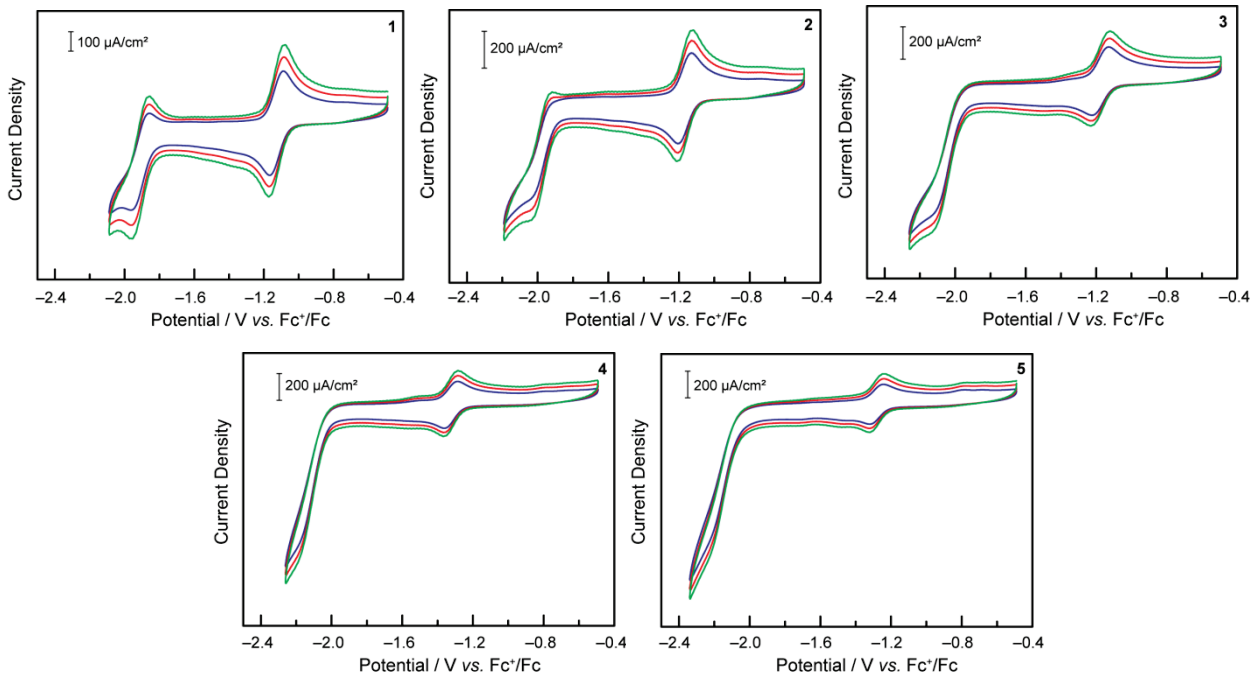

Figure S10. Cyclic voltammograms of 1 mM solutions of **1**, **2**, **3**, **4** and **5** in DMF/H_2O (95:5), $TBAPF_6$ 0.1M, on a glassy carbon electrode under CO_2 saturating conditions at a scan rate of 500 (— blue), 750 (— red) and 1000 (— green) mV/s.

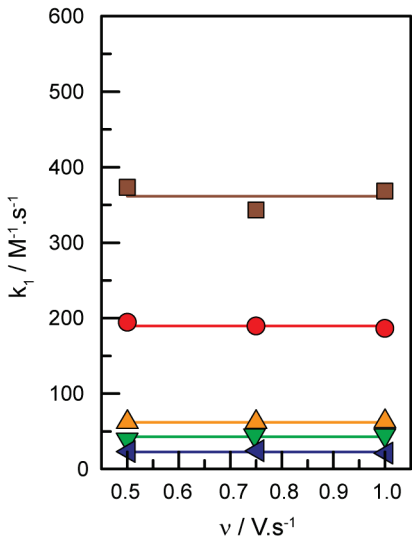

Figure S11. Estimated k_1 values obtained through the FOWA of compounds **1** (— blue), **2** (— green), **3** (— orange), **4** (— red) and **5** (— brown) at different scan rates under CO_2-saturating conditions using the CVs presented in Figure S9 and Figure S10.

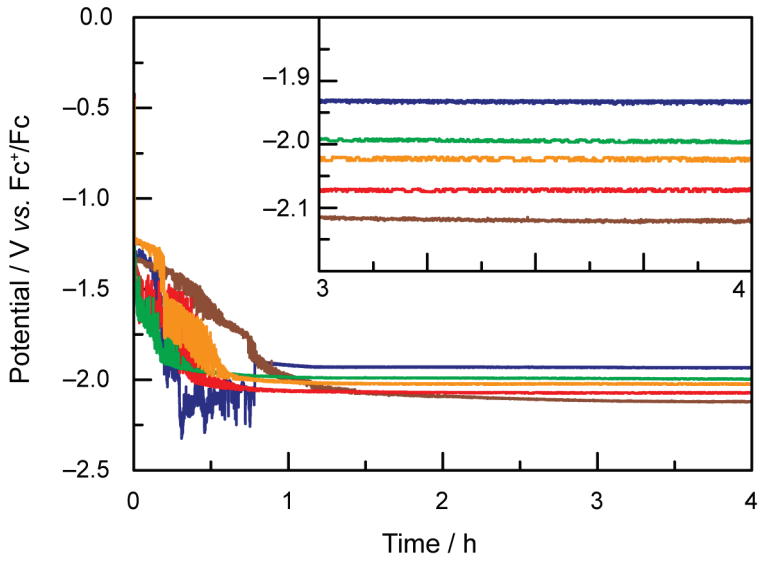

Figure S12. Potential observed during the bulk electrolysis of compounds **1** (— blue), **2** (— green), **3** (— orange), **4** (— red) and **5** (— brown) at a constant applied current of I = –300 μA. The bulk electrolyses were performed in 8 mL of DMF/H_2O (95:5, v:v), with 0.1 M $TBAPF_6$ as supporting electrolyte, using a 1.5 cm diameter pool of mercury as the working electrode. The concentration of **1**-**5** was 1 mM and the solutions were thoroughly degassed and saturated with CO_2. The cell used is described in Figure S15. Data was recorded every 0.05 s and the potential data was smoothed using an adjacent-averaging method over 5 s.

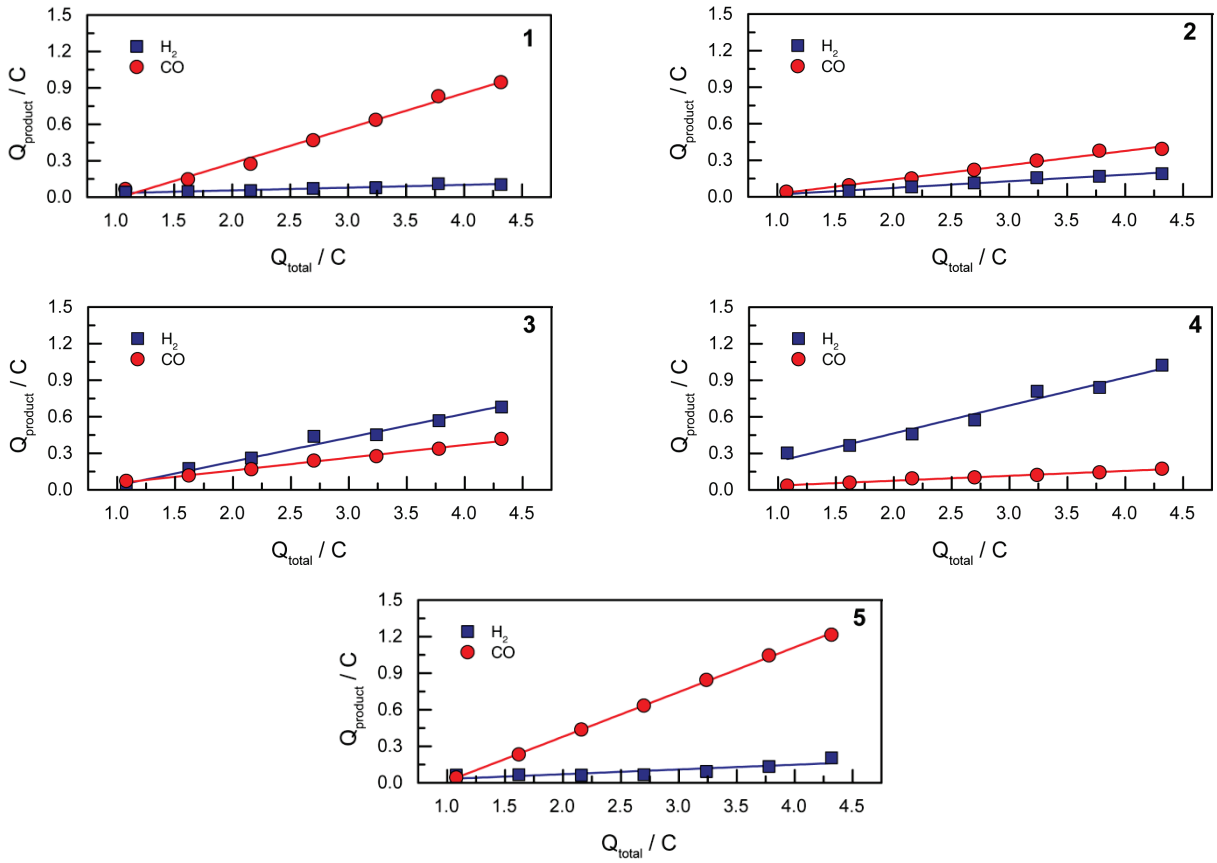

Figure S13. Charge corresponding to the products measured (H_2: ■ blue squares, CO: ● red circle) *vs.* the total charge passed during the electrolyses of **1**-**5** as described in Figure S12. The slopes of the linear fits, corresponding to the faradic efficiencies, are given in Fig. 7 of the main text.

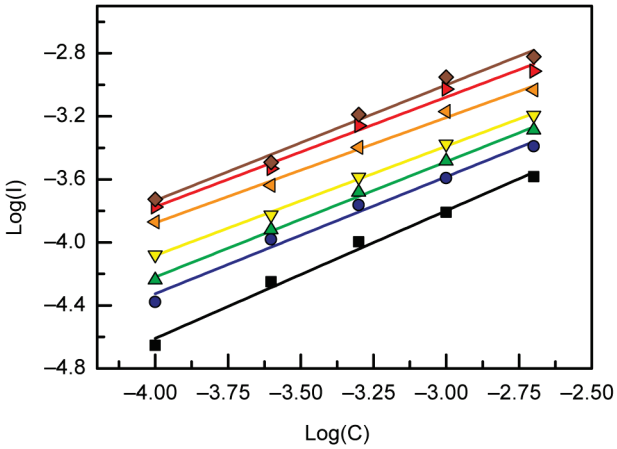

Figure S14. Plot of the log(current(A)) *vs.* the log(concentration(mol/L)) obtained in 5 controlled-potential electrolyses of **5** CO_2-saturated solutions at different concentrations of **5** where the potential was first held at –2.14 V *vs.* Fc^+/Fc until the current reached the plateau region and then varied in a step manner and the plateau current at each potential was recorded (brown diamonds: –2.29 V, red right triangles: –2.24 V, orange left triangles: –2.19 V, yellow down triangles: –2.14 V, green top triangles: –2.11 V, blue circles: –2.09 V, black squares: –2.06 V). Bulk electrolyses were performed in 8 mL of DMF/H_2O (95:5, v:v), with 0.1M $TBAPF_6$, using a 1.5 cm diameter pool of mercury as the working electrode. In an effort to reach conditions close to activation controlled, the solution above the pool of mercury was stirred as vigorously as possible without disrupting the surface of the mercury electrode. The cell used is described in Figure S15. Current values were corrected for the values observed in a solution without **5**, at each given potential. The slope of the linear fits, corresponding to the apparent order in **5** under bulk electrolyses conditions, is given in the table. Despite the efforts to be in conditions as close to activation control as possible in the setup, we cannot rule out a small contribution of diffusion limited conditions, which would contribute to an apparent order smaller than in reality. Keeping this in mind, the data is more representative of a behaviour that is 1st order in catalyst.

Applied potential	Apparent order in Cobalt	correlation coefficient
–2.29 V	0.73	0.980
–2.24 V	0.70	0.982
–2.19 V	0.67	0.990
–2.14 V	0.69	0.997
–2.11 V	0.73	0.996
–2.09 V	0.74	0.981
–2.06 V	0.81	0.987

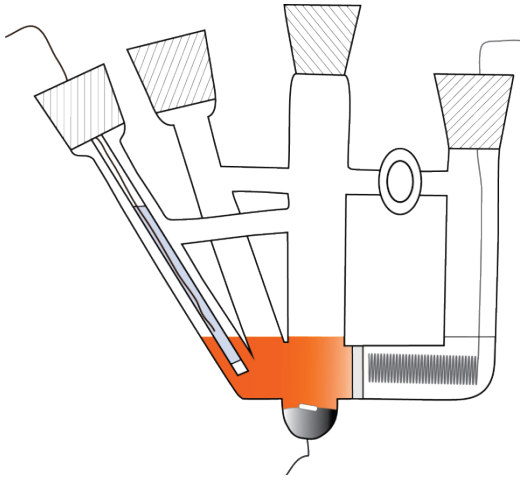

Figure S15. Schematic representation of the electrochemical cell used for bulk electrolyses (Reproduced from Ref. 16 of the main text with permission from the PCCP Owner Societies). The working compartment (8 mL, orange), on the left, contains the 1.5 cm diameter pool of mercury used as working electrode and the Ag/AgCl, 3M NaCl reference electrode. The working and reference electrodes are separated from the coiled platinum wire counter electrode by a porous glass frit. The solution is constantly stirred with a small stir bar floating over the pool of mercury. The electrochemical cell is gas tight, and the headspace can be sampled through rubber septa using gas tight syringes for gaseous products analyses.

Evaluation of Rate Determining Step

The mechanistic models proposed within Scheme 2 of the main text imply two possible rate determining steps (RDS). The first possible RDS is the protonation of a Co^0 centre to yield a Co^{II}–H and is governed by the rate constant k_1. The second possibility is that the RDS is the protonation of a Co–H to yield H_2, which proceeds at a rate constant defined as k_2. Rate limiting electron transfer is not considered as electron transfer is assumed to be fast.

As described in the main text, the *FOWA* affords a direct measurement of k_1 but does not provide information in regards to k_2 or the rate constant for the RDS (k_{cat}). Cyclic voltammograms are often used to estimate k_{cat} through comparison between catalytic plateau current (i_c) and the peak current in the absence of substrate (i_p^0). In both mechanisms considered in Scheme 2, i_c/i_p^0 is given by the following equation (reference 35 of the main text):

$$\frac{i_c}{i_{p^0}} = \frac{2}{0.4463}\frac{\sqrt{RT}}{\sqrt{F\nu}} \times \sqrt{[H^+]} \times \sqrt{k_{cat}} \qquad \textbf{(S1)}$$

As the experimental CV's for compounds **1**-**5** do not provide a catalytic plateau current that can be interpreted with a high degree of quantitative accuracy, we sought an alternate method to differentiate between k_1 and k_2 as the rate constant for the RDS. Given that k_1 is experimentally determined, using k_1 as k_{cat} we can estimate a maximum value for i_c/i_p^0 using equation S1. Additionally, setting the condition that if k_2 is the RDS, then $k_1 >> k_2$, we can estimate that a maximum value of k_2 is approximately $k_1/10$. Therefore, we can calculate a maximum theoretical value for i_c/i_p^0 in the scenario wherein k_2 is the RDS by substituting $k_1/10$ for k_{cat} into equation S1. Using **3** as an example, these estimates were made in Figure S16 with various scan rates analysed. The maximum i_c/i_p^0 values for $k_1 = k_{cat}$ is shown in red and the maximum i_c/i_p^0 values for $k_2 = k_{cat}$ is shown in blue. For illustrative purposed, if $k_2 = k_1/20 = k_{cat}$, the resulting i_c/i_p^0 values are shown in green.

With the theoretical boundary conditions calculated, we then estimated the experimental i_c/i_p^0 values for **3** at various scan rates. Of note, as no catalytic plateau is observed these estimates are likely underestimates. The experimental i_c/i_p^0 data is plotted in Figure S16 as a dashed black line. Upon comparing the experimental data to the theoretical boundaries established for $k_1 = k_{cat}$ and $k_2 = k_{cat}$, it is clearly observed that the empirical i_c/i_p^0 values are greater than the maximum theoretical values for $k_2 = k_{cat}$. Additionally, the empirical data is less than the theoretical maximum values for $k_1 = k_{cat}$. Given that the data is likely an underestimate, these results strongly suggest that the RDS is governed by k_1 and that the RDS is the protonation of the Co^0 complex.

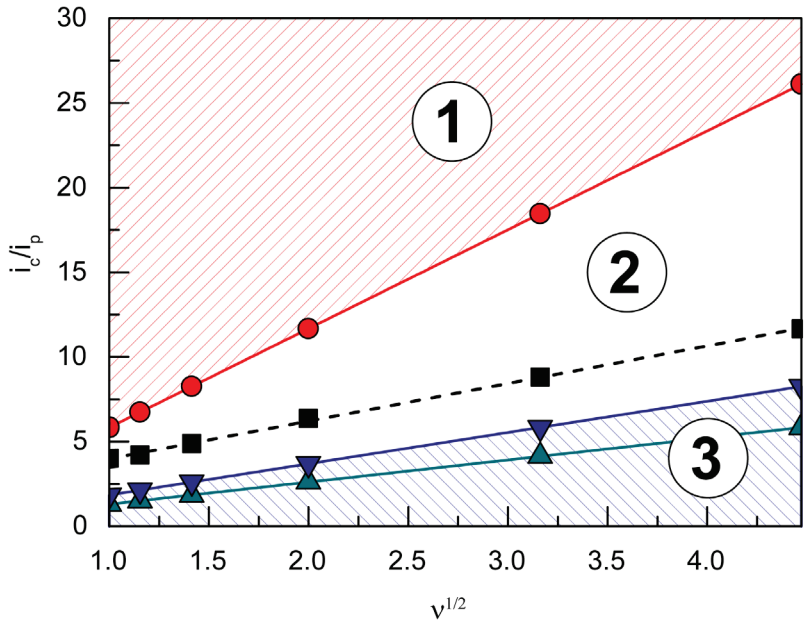

Figure S16. Theoretical values for i_c/i_p^0 for **3** in the presence of 60 mM acetic acid and various scan rates plotted using equation S1. Red circles represent values were $k_{cat} = k_1 = 1100$ $M^{-1}sec^{-1}$. Blue triangles represent values were $k_{cat} = k_2 = k_1/10 = 110$ $M^{-1}sec^{-1}$. Green triangles represent values were $k_{cat} = k_2 = k_1/20 = 55$ $M^{-1}sec^{-1}$. There exist three distinct regions of the plot. Region 1 includes all values of i_c/i_p^0 that are theoretically impossible to obtain as they are greater than the maximum possible values based on $k_1 = k_{cat}$. Region 2 represents values of i_c/i_p^0 that are indicative of k_1 being rate limiting, as they are below the maximum theoretical values for $k_{cat} = k_1$ but above the maximum theoretical values for $k_{cat} = k_2$. Region 3 represents values of i_c/i_p^0 where no statement can be made regarding the nature of the rate determining step, as values are both below the maximum theoretical values for $k_{cat} = k_1$ and $k_{cat} = k_2$. The experimentally estimated values for i_c/i_p^0 are plotted at the dashed line and clearly fall within Region 2. This strongly indicates that the rate determining step is governed by k_1.